Phase segregation in Pb:GeSbTe chalcogenide system

J. Kumar[1], M. Ahmad[1], R. Chander[1], R. Thangaraj[1,a], and T.S. Sathiaraj[2]

[1] Semiconductors Laboratory, Department of Applied Physics, Guru Nanak Dev University, Amritsar-143005, India
[2] Department of Physics, University of Botswana, Botswana

Received: 28 May 2007 / Received in final form: 12 July 2007 / Accepted: 4 October 2007
Published online: 19 December 2007 – © EDP Sciences

Abstract. Effect of Pb substitution on the amorphous-crystalline transformation temperature, optical band gap and crystalline structure of $Ge_2Sb_2Te_5$ has been studied. In Pb:GeSbTe chalcogenide films prepared by thermal evaporation, an amorphous to crystallization transition is observed at 124, 129, 136 and 138 °C in $Pb_9Ge_{20}Sb_{24}Te_{56}$, $Pb_{1.6}Ge_{19}Sb_{26}Te_{54}$, $Pb_3Ge_{17}Sb_{28}Te_{53}$ and $Pb_5Ge_{12}Sb_{28}Te_{55}$ respectively. XRD investigations of annealed samples reveal that Pb substitution retains NaCl type crystalline structure of GST but expands the lattice due to large atomic radii. The increase in amorphous-crystalline transformation temperature is followed with the increase in phase segregation. The optical gap shows marginal variations with composition.

PACS. 61.66.Dk Alloys – 61.72.Ww Doping and impurity implantation in other materials – 73.61.Jc Amorphous semiconductors; glasses – 84.37.+q Measurements in electric variables

1 Introduction

Chalcogenide materials produced by rapid quenching are used in numerous applications including photovoltaic devices, infrared windows and infrared filters [1–3]. One of the major applications of chalcogenide glasses is in phase change memory devices. The idea to use these materials for memory devices, originated when Stanford R. Ovshinsky suggested using differences in electrical and optical properties between amorphous and crystalline phases of Te based chalcogenides for data storage [4]. $Ge_2Sb_2Te_5$ (GST) is of great interest because of its extensive use in phase change memories (PCM) [5,6]. Due to its (i) faster crystallization, (ii) reflectivity and large resistivity difference between amorphous and crystalline states, GST finds application in DVD-RAM and PCRAM [7–9]. Amorphous-crystalline transformation in GST is fast and stable due to the absence of the rupture of strong covalent bonds during the above process. The Te sublattice as well as the structure around Sb atoms is partially preserved in the amorphous state [10]. Many researchers have made efforts to improve the phase change characteristics of GST [7,11–14]. Doping of Bi or Sn to GST has been found to reduce the amorphous-crystalline transformation temperature (T_c) and improve the speed of recrystallization (<10 ns) [6,12,14]. Retarded crystallization has been reported with In doping [13]. In addition to other metallic impurities, Pb has also been considered as a good dopant in chalcogenide materials [15,16]. Pb belongs to the same group as that of the Ge and its partial substitution for Ge may lead to materials with desirable phase change properties.

However, the effect of Pb doping on GST has not been investigated till now. In this work, we describe the investigation of the amorphous-crystalline transformation in Pb doped GST using electrical, optical and X-ray measurements.

2 Experimental

Bulk $Pb_xGe_{22-x}Sb_{22}Te_{55}$ ($x = 0$, 1, 2, 3) alloys were prepared by melt quenching technique. The constituent elements (99.999% purity) were weighed according to their atomic percentage and were sealed in a quartz ampoule (length ∼10 cm, internal diameter ∼6 mm), in the vacuum of $\sim 10^{-5}$ mbar. The sealed ampoule was kept in a vertical furnace for 48 h and the temperature was raised to 1000 °C, at a rate of 4–5 °C/min. The ampoule was rocked constantly to ensure homogeneous mixing of the melt. Finally, the ampoule containing molten alloy was quenched in ice-cold water. The bulk material was extracted from quartz ampoule by dissolving the ampoule in $HF + H_2O_2$ solution for about 48 h. Ingot so obtained was crushed into fine powder.

Thin films of the above-mentioned Pb:GeSbTe alloys were prepared by thermal evaporation method using Hind High Vacuum Coating Unit (Model No. 12A4D). Well-cleaned glass slides were used as substrates. The substrates were maintained at room temperature during deposition and the pressure in the chamber during the

[a] e-mail: rthangaraj@rediffmail.com

Table 1. The at.% of Pb, Ge, Sb and Te in different samples calculated from EDAX data.

Samples with initial compositions	Thickness of thin films (Å)	Elements	Spot1 (At.%)	Spot2 (At.%)	Spot3 (At.%)	Average (At.%)	Samples with actual compositions
$Pb_0Ge_{22}Sb_{22}Te_{56}$	7143	Ge	20.25	20.1	19.42	19.92	$Pb_0Ge_{20}Sb_{24}Te_{56}$
		Sb	24.13	24.46	24.52	24.37	
		Te	55.62	55.44	56.05	55.71	
$Pb_1Ge_{21}Sb_{22}Te_{56}$	8152	Pb	1.71	1.58	1.48	1.59	$Pb_{1.6}Ge_{19}Sb_{26}Te_{54}$
		Ge	19.57	18.08	18.13	18.59	
		Sb	26.03	26.87	26.14	26.35	
		Te	52.69	53.48	54.25	53.47	
$Pb_3Ge_{21}Sb_{22}Te_{56}$	7412	Pb	2.38	2.78	2.95	3.04	$Pb_{3.0}Ge_{17}Sb_{28}Te_{53}$
		Ge	16.27	17.42	16.69	16.79	
		Sb	27.84	27.84	28.32	28	
		Te	52.5	51.96	52.04	52.17	
$Pb_5Ge_{11}Sb_{22}Te_{56}$	8656	Pb	5.04	5.14	4.99	5.06	$Pb_5Ge_{12}Sb_{28}Te_{55}$
		Ge	11.65	11.69	12.4	11.91	
		Sb	27.65	27.67	27.24	27.52	
		Te	55.66	55.5	55.37	55.51	

deposition was below 10^{-5} mbar. The films were left inside the vacuum chamber after deposition for ~24 h to attain metastable equilibrium as-suggested by Abkowitz [17]. Thickness of the as deposited films was measured using (KLA Tencor P15) surface profiler. The crystal structure of the as-deposited and annealed thin films was identified using a Philips X-ray diffractometer (PW3710 mpd controlled XRD system with a PW1830 generator). The chemical compositions were determined using EDAX attached with Scanning Electron Microscope (Philips XL 30 ESEM system). The average composition of each thin film was obtained by measuring three regions of the thin film. For resistivity measurements, Al electrodes were deposited in coplanar geometry with a gap of ~2 mm. The amorphous-crystalline transformation temperatures of the alloys were determined by temperature dependent resistivity measurements. The temperature at which an abrupt drop in the resistivity takes place was taken as the amorphous crystalline transformation temperature. The transmittance (T) w.r.t. air and specular reflectance (R) of thin films were measured at room temperature using UV-VIS-NIR spectrophotometer (VARIAN Cary 500) in the wavelength range 200–3000 nm.

3 Results and discussion

3.1 Compositional analysis

The compositions of different films represented as A, B, C and D corresponding to Pb_0Ge_{20} $Sb_{24}Te_{56}$, $Pb_{1.6}Ge_{19}Sb_{26}Te_{54}$, $Pb_3Ge_{17}Sb_{28}Te_{53}$ and Pb_5Ge_{12} $Sb_{28}Te_{55}$ respectively are shown in Table 1. From the table, it is observed that the ratio of Ge/Sb in thin films is lower as compared to the initial composition taken for the preparation of bulk material. The Ge/Sb ratio also decreases with addition of Pb. This change in the relative composition leads to deficiency of Ge to form stoichiometric GST.

With the presence of excess Sb and Te, the possible phases with their priority of formation are analyzed using the chemically ordered network (CON) model. According to this model, the formation of heteropolar bonds is preferred to the homopolar bonds. In this model, the glass structure is assumed to be composed of cross-linked structural units of the stable compounds (heteropolar) [18]. The bond energy values of different bonds Ge-Ge, Sb-Sb, Te-Te, Pb-Pb, Ge-Te, Sb-Te and Pb-Te expected in present system are 263.6, 299.2, 259.8, 86.6, 456, 277.4 and 251 kJ/mol respectively [19]. Among the different bonds, the stronger Ge-Te bonds are favored over the weaker Sb-Te bonds and Sb-Te bonds have priority over all other bonds. The possible phases are shown in Table 2. The pseudo binary $Ge_2Sb_2Te_5$ phase decreases whereas, the Sb_2Te_3 phase increases from compositions A to D. Pb shows the monotonic increase from B to D. The excess of Te atoms in composition D are responsible for the Pb-Te phase in this composition.

3.2 Resistivity measurements

Figure 1 shows the resistivity values of Pb_0Ge_{20} $Sb_{24}Te_{56}$, $Pb_{1.6}Ge_{19}Sb_{26}Te_{54}$, $Pb_3Ge_{17}Sb_{28}Te_{53}$ and Pb_5Ge_{12} $Sb_{28}Te_{55}$ films, at a heating rate of 2 °C/min. A continuous decrease in resistivity is observed followed by an abrupt drop at 124, 129, 136 and 138 °C for $Pb_0Ge_{20}Sb_{24}Te_{56}$, $Pb_{1.6}Ge_{19}Sb_{26}Te_{54}$, $Pb_3Ge_{17}Sb_{28}Te_{53}$ and $Pb_5Ge_{12}Sb_{28}Te_{55}$ films respectively. The presence of the abrupt drop in resistivity with temperature variation is characteristic of GST system and indicates that the GST is present as a continuous network in the whole of the sample and is mainly responsible for electrical conduction. The model presented by Kolobov et al. provide a clear explanation of rapid amorphous-crystalline transformation in GST [10]. In $Ge_2Sb_2Te_5$, Te atoms form fcc lattice and Ge occupies octahedral and tetrahedral positions in the crystalline and amorphous states respectively.

Table 2. Possible number of molecules for different phases with preference of formation.

Phases	Possible number of molecules of different phases with preference of formation			
	A	B	C	D
$Ge_2Sb_2Te_5$	9.96	9.3	8.4	5.96
Sb_2Te_3	1.97	2.32	3.4	7.8
Pb-Te	-	-	-	2.31
Sb	0.51	3.11	4.41	-
Pb	-	1.59	3.04	2.75

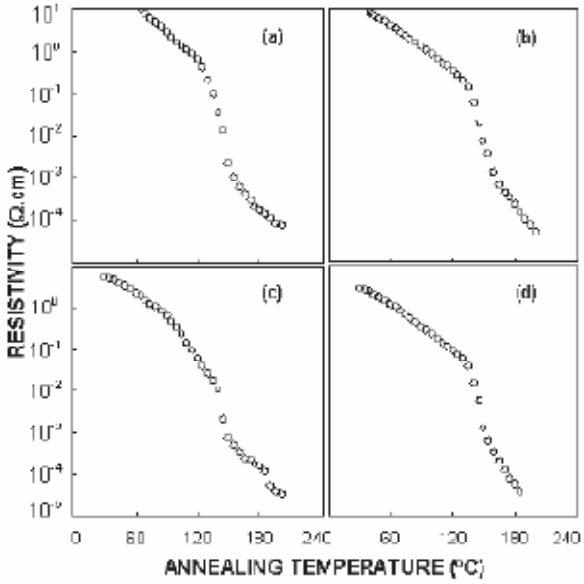

Fig. 1. Resistivity variation with temperature in (a) $Pb_0Ge_{20}Sb_{24}Te_{56}$, (b) $Pb_{1.6}Ge_{19}Sb_{26}Te_{54}$, (c) $Pb_3Ge_{17}Sb_{28}Te_{53}$, (d) $Pb_5Ge_{12}Sb_{28}Te_{55}$ films.

At amorphous to crystalline transformation temperature, with the rupture of weak bonds Ge flips into the tetrahedral position. Whereas on melting the Ge atom undergoes a reverse (umbrella) flip to octahedral position resulting in the distortion of the Ge sublattice [8]. This rapid amorphous-crystalline transformation appears as an abrupt drop in resistivity in temperature dependent resistivity measurements, which has been further confirmed by XRD studies reported in next section. The reduction in resistivity upon phase change is more than three orders of magnitude in every case. The local arrangement of atoms around Sb remains essentially unchanged. The Sb atoms mainly play the role of enhancing overall stability of the metastable crystal structure by participating in the overall electron balance [8].

3.3 X-ray diffraction studies

The analysis of the X-ray diffraction data provides deeper understanding of the observed amorphous to crystalline transformation exhibited in the resistivity measurement. Figure 2 shows the diffractograms of as deposited and annealed $Pb_0Ge_{20}Sb_{24}Te_{56}$, $Pb_{1.6}Ge_{19}Sb_{26}Te_{54}$, $Pb_3Ge_{17}Sb_{28}Te_{53}$ and $Pb_5Ge_{12}Sb_{28}Te_{55}$ thin films. Absence of any sharp peak in curve (i) confirms the amorphous nature of all the as-deposited thin films. Films annealed at 160 °C for 10 min [curve (ii)] shows no peak which indicates that the films remain amorphous. Curve (iii) in the above figure shows the diffraction peaks of the films annealed at 225 °C for 10 min. The peaks (111), (200), (220) and (222) in $Pb_0Ge_{20}Sb_{24}Te_{56}$ can be identified with fcc structure of $Ge_2Sb_2Te_5$ [6]. In Figure 2b–2d decrease in intensity of peak (200) belonging to $Ge_2Sb_2Te_5$confirm the decrease in this phase. While in Figure 2c, 2d few new peaks (105) (1010) and (205) can be clearly observed in addition to previously discussed peaks, the intensity of these peaks also increases as the at% of Ge decreases from 17 to 12. These peaks are identified as Sb_2Te_3 peaks. The value of the lattice parameter determined from the X-ray diffraction data for NaCl type fcc structure of $Pb_0Ge_{20}Sb_{24}Te_{56}$is 6.002 ± 0.004 Å which is in good agreement with the reported value for undoped $Ge_2Sb_2Te_5$ [19]. For $Pb_{1.6}Ge_{19}Sb_{26}Te_{54}$, $Pb_3Ge_{17}Sb_{28}Te_{53}$ and $Pb_5Ge_{12}Sb_{28}Te_{55}$ films the value of the lattice parameter is determined to be 6.066 ± 0.001, 6.112 ± 0.005 and 6.185 ± 0.009 Å respectively, which is marginally higher than that for the undoped GST. Diffraction scans shown in curve (iii) of Figure 2d, new peaks corresponding to (105), (1010) and (205) diffraction planes, indicates the formation of weaker Sb-Te bonds at the expense of stronger Ge-Te bonds. Occupation of a Ge site over the Pb or Te site by Sb is favored because Sb forms stronger bond with Te. The bond energy of Pb-Te is less than Sb-Te, which is further less than Ge-Te. This results in an increase in the dominance of the Sb_2Te_3 phase with increasing Pb substitution. The increased dominance of the Sb_2Te_3 phase over stoichiometric $Ge_2Sb_2Te_5$ causes phase segregation in these compositions. This is similar to the one observed in InGeSbTe system [12]. The increase in the Sb_2Te_3 phase, i.e., increase in phase segregation must be responsible for the increase in amorphous-crystalline transformation temperature Table 3. Compositional analysis showed the possibility of formation of Pb-Te phase for composition D, because of very small concentration left after formation of the $Ge_2Sb_2Te_5$ and Sb_2Te_3 phase, a small tip of peak (200) belonging to the Pb-Te phase is observed (Fig. 2d).

3.4 Optical properties

The absorption coefficient (α) of the films has been calculated from the transmission and reflection data using the

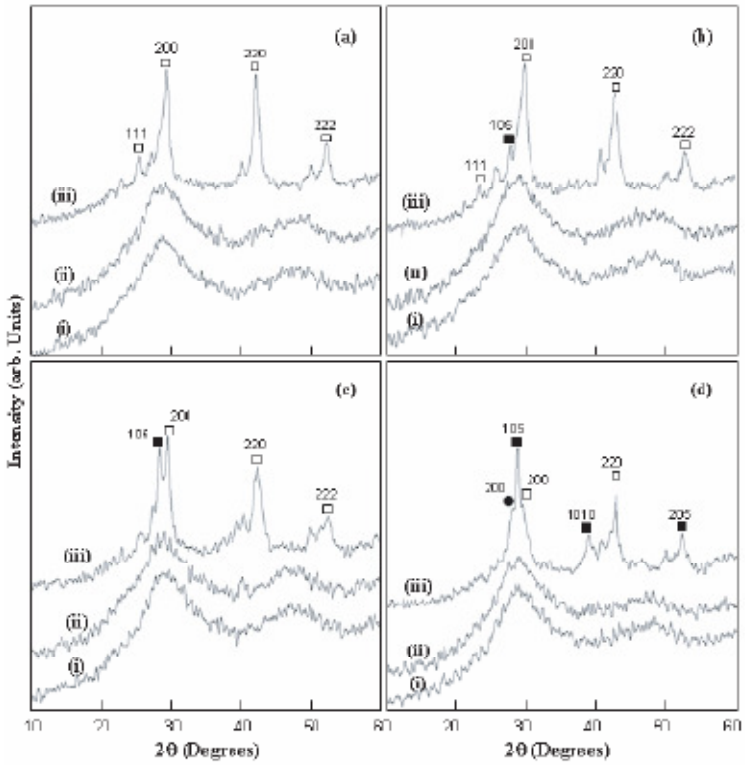

Fig. 2. XRD scans of (a) $Pb_6Ge_{23}Sb_{24}Te_{53}$, (b) $Pb_{1.6}Ge_{19}Sb_{26}Te_{54}$, (c) $Pb_3Ge_{17}Sb_{28}Te_{53}$, (d) $Pb_5Ge_{12}Sb_{28}Te_{55}$films. (Curve (i), as-deposited; curves (ii) and (iii), annealed for 10 min. at 160 and 225 °C respectively; (□) fcc, phase of $Ge_2Sb_2Te_5$, (■) Sb_2Te_3 phase and (•) fcc PbTe phase).

Table 3. Amorphous-crystalline transformation temperature, tailing parameter and optical gap for Pb:GeSbTe.

Compositions	A	B	C	D
T_c (°C)	124	129	136	138
B^{-1}(cm eV)	1.96	1.96	2.01	2.09
E_o (eV)	0.43	0.44	0.36	0.39

relation [21]

$$\alpha = \left(\frac{1}{t}\right) \ln\left\{\frac{(1-R^2)}{(2T)} + \left\{\frac{(1-R)^2}{(2T)^2} + R^2\right\}^{1/2}\right\} \quad (1)$$

where 't' is the thickness of the films. 'T' and 'R' represent transmission and reflection percentage respectively.

According to Tauc [22] it is possible to separate three distinct regions in the absorption edge spectrum of amorphous semiconductors. The first is the weak absorption tail, which originates from defects and impurities, the second is the exponential edge region, which is strongly related to the structural randomness of the system and the third is the high absorption region that determines the optical energy gap. In the high absorption region, involving indirect interband transitions between valence and conduction bands, α follows the relation:

$$\alpha = B(h\nu - E_0)^2/h\nu. \quad (2)$$

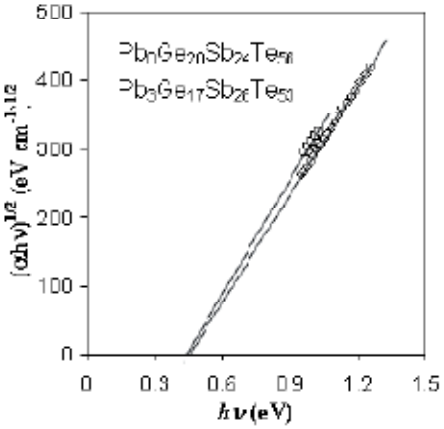

Fig. 3. Plots of $(\alpha h\nu)^{1/2}$ vs. $h\nu$ for (◊) $Pb_0Ge_{20}Sb_{24}Te_{56}$ and (□) $Pb_3Ge_{17}Sb_{28}Te_{53}$ films.

where E_0 is the optical band gap and B is a constant, which is a measure of the extent of band tailing [22]. A plot of $(\alpha h\nu)^{1/2}$ versus $h\nu$ gives a straight line, whose intercept on the energy axis gives E_0 and whose slope gives the value of constant B^{-1}. Plots of $(\alpha h\nu)^{1/2}$ versus $h\nu$ for various compositions are shown in Figure 3. The calculated values of the optical band gap E_0 and the approximate values of the band tailing parameter B^{-1} are shown in Table 3. It can be observed form Table 3, that B^{-1} increases and E_0 decrease as the composition changes from A to D. However, the charges in the above parameters are only marginal.

Ming and Fang et al. reported that optical band gap for as-deposited GST films increase with the increasing film thickness (E_0 = 0.81 eV for 127 nm, E_0 = 0.68 eV for 57 nm thin films) [21]. Thus, the optical gap of ~780 nm thick film must remain above 0.81 eV, which is not observed for the analyzed compositions A to D. Further, the E_0 for Ge-Te reported by Dangol is between 1–2 eV, which is still higher than ours [23]. The E_0 for Sb_2Te_3 is 0.28 eV, which is near to the observed values in our case [24]. It confirms that the optical band gap in our films is dominated by Sb_2Te_3 in all compositions.

Pb substitution does not show any considerable change in optical properties. But, substitution of Pb in place of Ge leads to decrease in the $Ge_2Sb_2Te_5$ phase, which is confirmed by XRD data of annealed films. The increase in lattice constant value indicates expansion in $Ge_2Sb_2Te_5$ lattice with the addition of Pb. This means Pb must be entering the $Ge_2Sb_2Te_5$ lattice. The Sb_2Te_3 phase emerges as the second dominant phase, which is responsible for phase segregation and hence an increase in amorphous-crystalline transformation temperature. As observed in optical analysis, small change in the value of E_o indicates the dominance of the Sb_2Te_3 phase. The presence of (105), (1010) and (205) peaks further confirm the Sb_2Te_3 phase. Increase of Sb_2Te_3 peak confirms the increase in phase segregation from composition A to D.

4 Conclusion

A comparison of optical and phase change properties for undoped and Pb doped $Ge_{22}Sb_{22}T_{55}$ reveals that substitution of Pb expands the $Ge_2Sb_2Te_5$ lattice. Sb_2Te_3 segregates as a second phase due to the deficiency of Ge and excess of Sb and increases with an increase of Pb. The increased phase segregation is responsible for the increasing amorphous-crystalline transformation temperature. The presence of abrupt change in resistivity indicates the role of the $Ge_2Sb_2Te_5$ phase in electrical properties. A marginal change in the value of E_0 shows the dominance of the Sb_2Te_3 phase.

References

1. B. Bureau, X.H. Zhang, F. Smektala, J.L. Adam, J. Troles, H. Ma, C.B. Pledel, J. Lucas, P. Lucas, D.L. Coq, M.R. Riley, J.E. Simmons, J. Non-Cryst. Solids **345**, 276 (2004)
2. A. Seddon, J. Non-Cryst. Solids **184**, 44 (1995)
3. J.L. Adam, J. Non-Cryst. Solids **287**, 401 (2001)
4. S.R. Ovshinsky, Phys. Rev. Lett. **21**, 20 (1968)
5. N. Yamada, E. Ohno, K. Nishiuchi, N. Akahira, J. Appl. Phys. **69**, 2849 (1991)
6. S. Gu, L. Hou, Q. Zhao, R. Huang, Chin. Opt. Lett. **1**, 716 (2003)
7. S.W. Ryu, J.H. Oh, E.J. Choi, S.V. Hwang, S.K. Hong, C.S. Hwang, H.J. Kim, Electrochem. Solid-State Lett. **9**, G259 (2006)
8. A.V. Kolobov, P. Fons, J. Tominaga, A.I. Frenkel, A.L. Ankudinov, S.N. Yannopoulous, K.S. Andrikopoulos, T. Uruga, Jpn J. Appl. Phys. **44**, 3345 (2005)
9. M. Popescu, J. Optoelectron. Adv. Mater. **8**, 2045 (2006)
10. A.V. Kolobov, P. Fons, A.I. Frenkel, A.L. Ankudinov, J. Tominaga, T. Uruga, Nature Mater. **3**, 703 (2004)
11. X.J. Lin, L. Bo, S.Z. Tang, F.S. Lin, C. Bomy, Chin. Phys. Lett. **22**, 934 (2005)
12. K. Wang, D. Wamwangi, S. Ziegler, C. Steimer, M. Wuttig, J. Appl. Phys. **96**, 5557 (2004)
13. K. Wang, C. Steimer, D. Wamwangi, S. Ziegler, M. Wuttig, Appl. Phys. A **80**, 1611 (2005)
14. X. Cheng, L. Bo, S.Z. Tang, F.S. Lin, C. Bomy, Chin. Phys. Lett. **22**, 2929 (2005)
15. M.S. Kamboj, R. Thangaraj, Eur. Phys. J. Appl. Phys. **24**, 33 (2003)
16. L.A. Wahab, H.H. Amer, Egypt. J. Solids **28**, 255 (2005)
17. M. Abkowitz, Polym. Eng. Sci. **24**, 1149 (1984)
18. G. Lucovsky, F.L. Galeener, R.H. Geils, R.C. Keezer, *The Structure of Non-Crystalline Materials* (Taylor and Francis, London, 1977)
19. J.A. Kerr, *CRC Handbook of Chemistry and Physics* (CRC Press, Florida USA, 2000)
20. I. Friedrich, V. Wedenhof, W. Njoroge, P. Franz, M. Wuttig, J. Appl. Phys. **87**, 4130 (2000)
21. M. Fang, Q. Li, F. Cao, Chinese Opt. Lett. **2**, 177 (2004)
22. J. Tauc, *Amorphous and Liquid Semiconductors* (Plenum Press, London, 1974)
23. M. Dongol, Egypt. J. Sol. **23**, 297 (2000)
24. S.N. Dhar, C.F. Desai, Phil. Mag. Lett. **82**, 581 (2002)